Journal of Solid State Chemistry 182 (2009) 435–441

Contents lists available at ScienceDirect

Journal of Solid State Chemistry

journal homepage: www.elsevier.com/locate/jssc

Synthesis, characterization, and near-infrared luminescent properties of the ternary thulium complex covalently bonded to mesoporous MCM-41

Jing Feng [a,b], Shu-Yan Song [a,b], Yan Xing [a], Hong-Jie Zhang [a,*], Zhe-Feng Li [a,b], Li-Ning Sun [a], Xian-Min Guo [a,b], Wei-Qiang Fan [a,b]

[a] State Key Laboratory of Rare Earth Resource Utilizations, Changchun Institute of Applied Chemistry, Chinese Academy of Sciences, Changchun 130022, PR China
[b] Graduate School of the Chinese Academy of Sciences, Beijing, PR China

ARTICLE INFO

Article history:
Received 14 April 2008
Received in revised form
31 October 2008
Accepted 12 November 2008
Available online 21 November 2008

Keywords:
MCM-41
Thulium complex
Covalently bonded
Near-infrared luminescence
Optical telecommunication

ABSTRACT

The crystal structure of a ternary $Tm(DBM)_3phen$ complex (DBM = dibenzoylmethane; phen = 1, 10-phenanthroline) and the synthesis of hybrid mesoporous material in which the complex covalently bonded to mesoporous MCM-41 are reported. Crystal data: $Tm(DBM)_3phen$ $C_{59}H_{47}N_2O_7Tm$, monoclinic, $P21/c$, $a = 19.3216(12)$ Å, $b = 10.6691(7)$ Å, $c = 23.0165(15)$ Å, $\alpha = 90°$, $\beta = 91.6330(10)°$, $\gamma = 90°$, $V = 4742.8(5)$ Å^3, $Z = 4$. The properties of the $Tm(DBM)_3phen$ complex and the corresponding hybrid mesoporous material [$Tm(DBM)_3phen$-MCM-41] have been studied. The results reveal that the $Tm(DBM)_3phen$ complex is successfully covalently bonded to MCM-41. Both $Tm(DBM)_3phen$ complex and $Tm(DBM)_3phen$-MCM-41 display typical near-infrared (NIR) luminescence upon excitation at the maximum absorption of the ligands, which contributes to the efficient energy transfer from the ligands to the Tm^{3+} ion, an antenna effect. The full width at half maximum (FWHM) centered at 1474 nm in the emission spectrum of $Tm(DBM)_3phen$-MCM-41 is 110 nm, which is the potential candidate of broadening amplification band from C band (1530–1560 nm) to S^+ band (1450–1480 nm) in optical area.

1. Introduction

The trivalent lanthanide ions have been known for their unique optical properties such as line-like emission spectra and high-luminescence quantum efficiency [1]. Historically, detailed research has been almost exclusively devoted to europium and terbium luminescence [2–4]. In contrast, the NIR (near-infrared)-emitting lanthanide ions Er^{3+}, Nd^{3+}, Yb^{3+}, and especially Tm^{3+}, are less well studied. Recently, there is a strong interest in the development of optical amplifiers designed to cover a larger bandwidth than currently available. Optical properties of trivalent thulium doped inorganic materials have already been investigated in order to achieve NIR emission [5]. Especially in the case of 1.4 μm band emission of Tm^{3+} ions, being the potential candidates of broadening amplification band from C band (1530–1560 nm) to S^+ band (1450–1500 nm) in optical fiber, Tm^{3+} doped fiber amplifiers have been regarded as one of important components used in wavelength division multiplexing technology [6].

Unfortunately the lanthanide ions are characterized by very low absorption coefficients ($\varepsilon \leqslant 1\ M^{-1}\ cm^{-1}$), which makes it difficult to populate the emitting levels by direct excitation effectively [7]. To enhance absorption, lanthanide ions are chelated with organic ligands that have broad, intense absorption bands in the UV region. The ion-centered luminescence originates from the intramolecular energy transfer through the excited states of the ligand to the emitting level of the lanthanide ion. This is the so-called "antenna effect" [8–12].

For practical applications in optical devices, it is advantageous to incorporate these lanthanide complexes in an inert host matrix, for example, silica-based materials [13–17], polymers [18–20], or liquid crystal [21,22]. Since the mesoporous silica materials were first introduced in the early 1990s [23,24], the development of ordered mesoporous molecular sieves has been of widespread interest in material science. Ordered mesoporous with unique properties (e.g., high surface area, high pore volume, controlled pore structure, and uniform pore size distribution) are of great interest for adsorption, sensing, catalysis, and other applications [25–28]. Recently, one of particular interests is the use of the ordered mesoporous silica material as a support for lanthanide complexes. MCM-41, one member of the mesoporous materials family, M41S, contains a hexagonal arrays of one-dimensional channels of uniform mesopores with a pore diameter between 1.5 and 30 nm and tailorable interior surfaces [23,24]. This perfect periodic nanostructure renders it an ideal host for lanthanide complexes and lanthanide complexes coupled to ordered mesoporous materials via a covalently bonded group have already been reported [29–33]. Also, some organic chromophores grafted to mesoporous materials have been extensively described in recent

* Corresponding author. Fax: +86 431 85698041.
E-mail address: hongjie@ciac.jl.cn (H.-J. Zhang).

0022-4596/$ - see front matter © 2008 Elsevier Inc. All rights reserved.
doi:10.1016/j.jssc.2008.11.007

studies [34,35]. These studies indicate that the thermal stabilities and mechanical properties of lanthanide complexes and the organic chromophores were improved by the matrixes. In principle, lanthanide complexes and the organic chromophores can be dispersed and isolated from each other, which for some systems should minimize intermolecular quenching of luminescence properties. In fact, compared with physical doping method [36,37], this method enables a higher and more homogeneous surface coverage of organosilane functionalities and can effectively prevent the aggregation of emitting centers and the leaching of the photoactive molecules in the resultant materials. To our best knowledge, thulium complex has been rarely incorporated to mesoporous materials. In this work, we report the structure of $Tm(DBM)_3$phen complex and the syntheses of MCM-41 mesoporous material covalently bonded with Tm $(DBM)_3$phen complex via a functionalized 1,10-phenanthroline (phen) group 5-(*N*,*N*-bis-3-(triethoxysilyl)propyl)ureyl-1,10-phenanthroline (phen-Si). Full characterization and detailed studies of NIR-luminescence properties of the $Tm(DBM)_3$phen complex and $Tm(DBM)_3$phen-MCM-41 mesoporous material were investigated.

2. Experimental section

2.1. Materials

Tetraethoxysilane (TEOS, Aldrich), 3-(triethoxysilyl)propyl isocyanate (TCI), cetyltrimethylammonium bromide (CTAB, Aldrich), fuming nitric acid and anhydrous ethanol were used as received. 1, 10-Phenanthroline monohydrate (phen · H_2O, 99%, AR) and dibenzoylmethane (DBM, CP) were bought from Beijing Fine Chemical Co. (Beijing, China). The solvent chloroform ($CHCl_3$) was used after desiccation with anhydrous calcium chloride. Thulium oxide (Tm_2O_3, 99.99%) was purchased from Yue Long Chemical Plant (Shanghai, China). $TmCl_3$ ethanol solution (EtOH) was prepared as follows: Tm_2O_3 was dissolved in concentrated hydrochloric acid (HCl), and the surplus HCl was removed by evaporation. The residue was dissolved with anhydrous ethanol. The concentration of the Tm^{3+} ion was measured by titration with a standard ethylenediaminetetraacetic acid (EDTA) aqueous solution.

2.2. Synthesis of the $Tm(DBM)_3$phen complex

The $Tm(DBM)_3$phen complex was prepared according to the following process. DBM and phen in a stoichiometric molar ratio were dissolved in a suitable volume of anhydrous ethanol. Then, an appropriate amount of 1 M sodium hydroxide solution was added dropwise to the solution to adjust the pH value to approximately 8–9. A stoichiometric amount of $TmCl_3$ ethanol solution was then added dropwise to the solution under stirring. The molar ratio of Tm^{3+}/DBM/phen was 1:3:1. The resulting precipitates were collected by filtration and dried at 70 °C under vacuum. The $Tm(DBM)_3$phen complex was recrystallized from ethanol. Yellow block crystals suitable for X-ray single-crystal structural determination were grown from the mother liquor at room temperature. Anal. calcd.: C, 66.54%; H, 4.45%; N, 2.63%. Found: C, 66.50%; H, 4.39%; N, 2.61%.

2.3. Synthesis of phen functionalized MCM-41 mesoporous material (phen-MCM-41)

The starting reagent 5-amino-1,10-phenanthroline (denoted as phen-NH_2) was prepared according to the procedure described in the literature [38]. Phen-Si was synthesized by the reaction of phen-NH_2 and 3-(triethoxysilyl)propyl isocyanate in $CHCl_3$ as described in Ref. [39]. Then CTAB (1.1 g) was dissolved in concentrated $NH_3 \cdot H_2O$ (12 mL), to which deionized water (26 mL), TEOS (5.0 mL), and phen-Si (0.598 g) were successively added. The molar composition of the original synthetic mixture was 0.04 phen-Si:1.0 TEOS:0.139 CTAB:3.76 $NH_3 \cdot H_2O$:66.57 H_2O. The mixture was stirred for 7 h at room temperature and transferred into a Teflon bottle sealed in an autoclave, which was then heated at 90 °C for 24 h. Then the solid product was filtered, washed thoroughly using deionized water, and dried for 12 h at 60 °C. Removal of surfactant CTAB was conducted by acid/solvent extraction, using a solution of 400 mL of ethanol and 7.3 mL of aqueous HCl (37%) per 5 g of sample. The mixture was refluxed for 7 h, then filtered and washed with EtOH until the pH was neutral. The collected solid was dried at 60 °C for 12 h in a vacuum to give a yellow product.

2.4. Synthesis of the $Tm(DBM)_3(H_2O)_2$

An appropriate amount of 1.0 M sodium hydroxide solution was added dropwise to DBM ethanol solution under stirring to adjust the pH value to approximately 8–9. The $TmCl_3$ ethanol solution was added dropwise into this mixture under stirring with the molar ratio of Tm^{3+}/DBM being 1:3. The mixture was heated under reflux for 6 h and then cooled to room temperature. The precipitates were collected by filtration, washed with water and ethanol, and dried overnight at 70 °C under vacuum.

2.5. Synthesis of [$Tm(DBM)_3$phen] ternary complex covalently bonded to MCM-41 mesoporous material [denoted as $Tm(DBM)_3$phen-MCM-41]

The phen-MCM-41 was soaked in an excess of [$Tm(DBM)_3(H_2O)_2$] $CHCl_3$ solution [3 equiv of $Tm(DBM)_3(H_2O)_2$ per phen moiety] under stirring. The mixture was heated under reflux for 6 h, followed by filtration and extensive washing with $CHCl_3$ to remove the excess of $Tm(DBM)_3(H_2O)_2$. The resulting $Tm(DBM)_3$phen-MCM-41 sample was dried at 60 °C under vacuum.

2.6. X-ray diffraction crystallography

X-ray data for the selected crystal mounted on a glass fiber were collected with a CCD area detector with graphite-monochromated Mo-$K\alpha$ radiation. Reflections were collected with a Bruker SMART APEX detector and processed with SAINT from Bruker. Data were corrected for Lorentz and polarization effects. The structure was solved by direct methods and expanded using Fourier techniques. The non-hydrogen atoms for $Tm(DBM)_3$phen were refined anisotropically. The hydrogen atoms were included using a riding model. All calculations were performed using the SHELXL-97 crystallographic software package. Crystallographic data and structural refinements for compound $Tm(DBM)_3$phen are summarized in Table 1. CCDC-684787 [for $Tm(DBM)_3$phen] contain the supplementary crystallographic data for this paper. These data can be obtained free of charge from The Cambridge Crystallographic Data Centre via www.ccdc.cam.ac.uk/data_request/cif.

2.7. Characterization

The CHN elemental analyses were carried out on a VarioEL analyzer. Small-angle X-ray diffraction (XRD) patterns were recorded in the 2θ range of 1.0–8.0° with SIEMENS-D5005 X-ray diffractometer using Cu$K\alpha$ radiation ($\lambda = 1.5416$ Å) at 40 kV and

Table 1
Crystal data and structure refinement for $Tm(DBM)_3phen$ complex.

Empirical formula	$C_{59}H_{47}N_2O_7Tm$
Formula weight	1064.92
Temperature (K)	293(2)
Wavelength (Å)	0.71073
Crystal system	Monoclinic
Space group	$P21/c$
a (Å)	19.3216(12)
b (Å)	10.6691(7)
c (Å)	23.0165(15)
α (deg)	90
β (deg)	91.6330(10)
γ (deg)	90
Volume (Å^3)	4742.8(5)
Z	4
$D_{calcd.}$ (mg m^{-3})	1.491
Absorption coefficient (mm^{-1})	1.929
$F(000)$	2160
Crystal size (mm)	0.23 × 0.27 × 0.16
θ range (deg)	1.77 to 25.37
Reflns collected	24631
Unique reflns (R_{int})	8657 (0.0249)
Refinement method	full-matrix least-squares on F^2
Data/restraints/parameters	8657/3/634
GOF on F^2	1.066
R_1 [$I>2\sigma(I)$]	0.0266
wR_2 [$I>2\sigma$(I)]	0.0606
R_1 (all data)	0.0325
wR_2 (all data)	0.0633

200 mA. The mesostructure of the Tm(DBM)3phen-MCM-41 mesoporous material was characterized by a JEOL-2010 transmission electron microscope (TEM) with an accelerating voltage of 200 kv. Nitrogen (N_2) adsorption/desorption isotherms were measured by using a Nova 1000 analyzer with nitrogen. The samples were outgassed for 4 h at 120 °C before the measurements. Specific surface areas were calculated by the Brunauer–Emmett–Teller (BET) method and pore sizes by the Barrett–Joyner–Halenda (BJH) methods. Diffuse reflectance (DR) spectra were acquired from HITACHI U-4100 spectrophotometer with tungsten and deuterium lamps. The luminescence excitation and emission spectra were recorded by a HORIBA Jobin Yvon FluoroLog-3 spectrofluorometer equipped with a 450 W Xe-lamp as an excitation source and a liquid-nitrogen-cooled R5509-72 PMT as detector. The time-resolved measurements, were done by using the third harmonic (355 nm) of a Spectra-physics Nd:YAG laser with a 5 ns pulse width and 5 mJ of energy per pulse as the source, and the NIR emission lines were dispersed by the emission monochromator of the HORIBA Jobin Yvon FluoroLog-3 equipped with liquid-nitrogen-cooled R5509-72 PMT, and the data were analyzed with a LeCroy WaveRunner 6100 1 GHz Oscilloscope. The luminescence lifetimes were calculated by Origin 7.0 software package. All the above measurements were performed at room temperature.

3. Results and discussion

3.1. Crystal structure of $Tm(DBM)_3phen \cdot C_2H_5OH$ complex

Single crystal of $Tm(DBM)_3phen \cdot C_2H_5OH$ complex was obtained by recrystallization from its ethanol solution. The crystal structure of $Tm(DBM)_3phen \cdot C_2H_5OH$ with the numbering scheme is displayed in Fig. 1a. Important experimental parameters for the structure determinations are tabulated in Table 1. The central Tm^{3+} ion is coordinated by six oxygen atoms from three DBM ligands and two nitrogen atoms from the phen ligand. Thus, the Tm^{3+} ion exhibits a coordination number of eight. From the

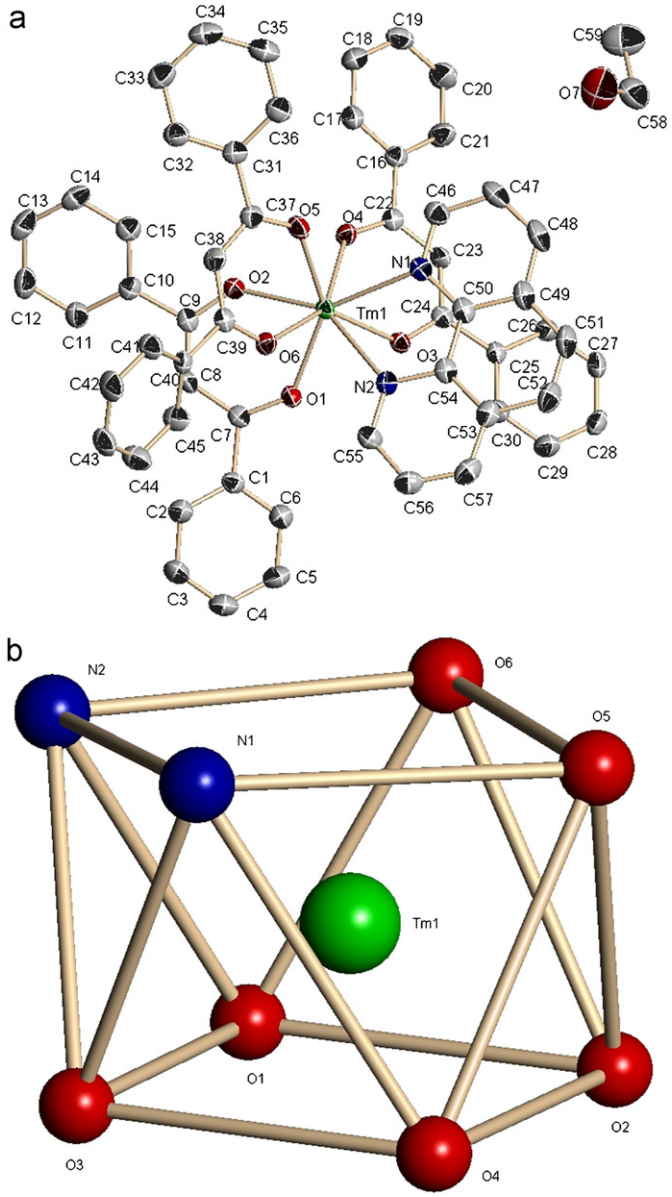

Fig. 1. (a) ORTEP plot for $Tm(DBM)_3phen \cdot C_2H_5OH$ with ellipsoids drawn at the 30% probability level. Hydrogen atoms were omitted for clarity and (b) coordination polyhedron of the Tm^{3+} ion.

coordination site angles, the coordination geometry of the central Tm^{3+} ion may be described as a square antiprism, one of the two most stable eight-coordinate polyhedra (shown in Fig. 1b). The average Tm–O distance is 2.294 Å and the average Tm–N distance is 2.545 Å. In the β-diketone rings of $Tm(DBM)_3phen$, the average distances for the C–C and C–O bonds are shorter than a single bond but longer than a double bond. This can be explained by the fact that there exists conjugated structure between the phenyl ring and the coordinated β-diketonate, which leads to the delocalization of electron density of the coordinated β-diketonate chelate ring. Also, the β-diketonate chelate ring itself is a conjugated structure due to the delocalization of electron density.

3.2. Small-angle XRD patterns and TEM images

The presence of the chelate ligand (phen-Si) covalently bonded to the mesoporous MCM-41 was confirmed by Fourier transform infrared (FTIR) and ^{29}Si MAS NMR spectroscopies, as we reported

previously [30,31]. In order to confirm the hexagonal mesostructures, the small-angle XRD patterns of the surfactant-extracted phen-MCM-41 and $Tm(DBM)_3$phen-MCM-41 mesoporous materials are compared in Fig. 2. These patterns feature distinct Bragg peaks in the 2θ range of 1–6°, which can be indexed as (100), (110), (200), and (210) reflections of a two-dimensional hexagonal ($p6mm$) structure of MCM-41 material. The values of the corresponding unit cell parameter a ($a = 2d_{100}/\sqrt{3}$) of phen-MCM-41 and $Tm(DBM)_3$phen-MCM-41 are 4.74 and 4.77 nm, respectively. Compared with that of phen-MCM-41 material (see Table 2), the d_{100} spacing value of $Tm(DBM)_3$phen-MCM-41 is nearly unchanged, indicating that the framework hexagonal ordering has been retained very well after the introduction of the $Tm(DBM)_3(H_2O)_2$ complex. It is also worth noting that the $Tm(DBM)_3$phen-MCM-41 material exhibit decreased diffraction intensity as compared to phen-MCM-41. This is probably due to the presence of $Tm(DBM)_3$phen inside the pore channels of $Tm(DBM)_3$phen-MCM-41 mesoporous material. Formation of well-defined 2D hexagonal Tm(DBM)3phen-MCM-41 was also confirmed by TEM as shown in Fig. 3. From the TEM images, we could find that the ordered mesostructure was still substantially conserved after the surfactant extraction procedure and the introduction of $Tm(DBM)_3(H_2O)_2$ complex. The hexagonal symmetry of $Tm(DBM)_3$phen-MCM-41 inferred from XRD is in agreement with TEM investigation.

3.3. Nitrogen adsorption/desorption isotherms

The N_2 adsorption/desorption isotherms for the surfactant-extracted phen-MCM-41 and $Tm(DBM)_3$phen-MCM-41 mesoporous materials are shown in Fig. 4. The isotherms of all materials display type IV isotherms according to the IUPAC classification [40], characteristic of MCM-41 mesoporous materials with highly uniform size distributions [41,42]. From the two branches of adsorption/desorption isotherms, the presence of a sharp adsorption step in the P/P_0 region from 0.2 to 0.4 shows that all materials possess a well-defined array of regular mesopores [43]. The specific area and the pore size are calculated by the BET method and BJH model, respectively. It is indicated that the BET method overestimates the surface area of MCM-41 [44]. The BET surface represents the total surface area rather than the mesopore area. However, it is a commonly used method to estimate the surface area of mesoporous materials. The BJH model is actually valid only for materials with pores >4 nm and underestimates the diameter of mesopores with pore diameters <4 nm by approximately 1 nm [45]. This is the weakness of BJH model to predict the critical size correctly when the hysteresis loop disappears [46]. However, it is a proper method for detecting changes in the pore-size

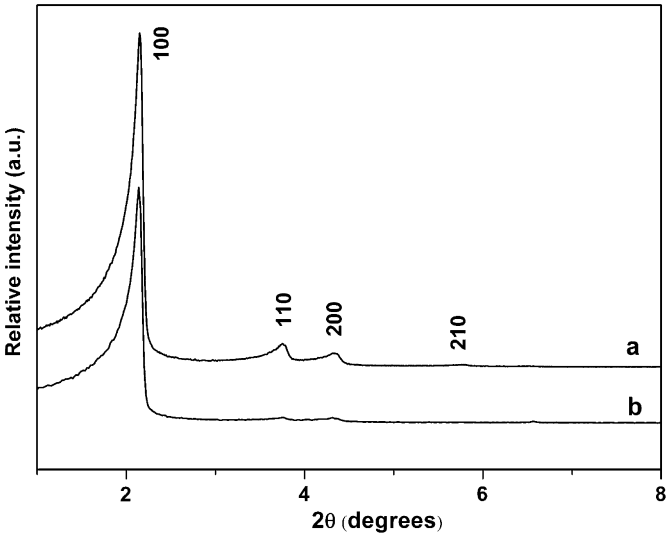

Fig. 2. XRD patterns of surfactant-extracted phen-MCM-41 (a), and $Tm(DBM)_3$phen-MCM-41 (b) mesoporous materials.

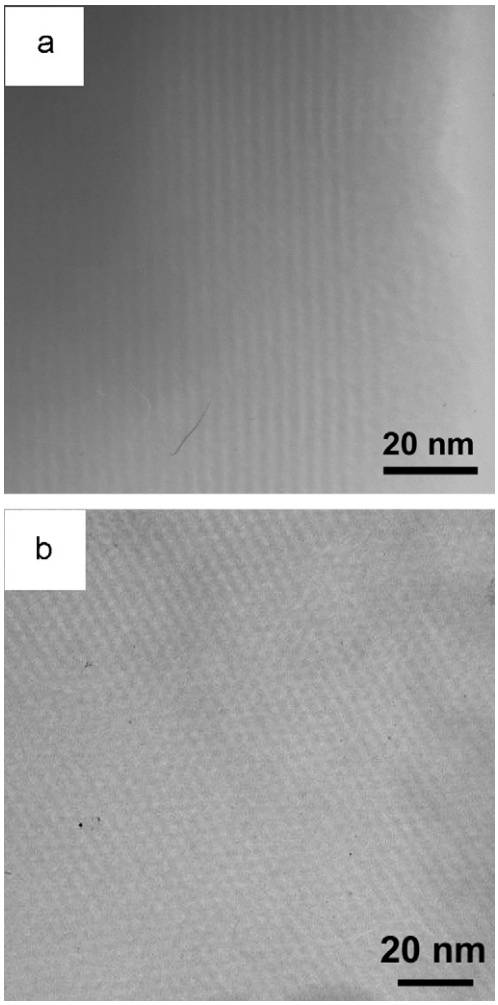

Fig. 3. TEM images of $Tm(DBM)_3$phen-MCM-41 recorded along: (a) parallel and (b) perpendicular to the pore axis.

Table 2
Textural parameters of phen-MCM-41, and $Tm(DBM)_3$phen-MCM-41[a].

Sample	d_{100} (nm)	a_0 (nm)	S_{BET} ($m^2 g^{-1}$)	V ($cm^3 g^{-1}$)	D (nm)	t (nm)
phen-MCM-41	4.11	4.74	973	1.05	2.79	1.95
$Tm(DBM)_3$phen-MCM-41	4.13	4.77	845	0.81	2.37	2.40

[a] d_{100} is the $d(100)$ spacing ($2d \sin\theta = k\lambda$; $k = 1$, $\lambda = 1.5416$ Å), a_0 the cell parameter ($a_0 = 2\, d_{100}/\sqrt{3}$), S_{BET} the BET surface area, V the total pore volume, D the average pore diameter calculated using BJH method, and t the wall thickness, $t = a_0 - D$.

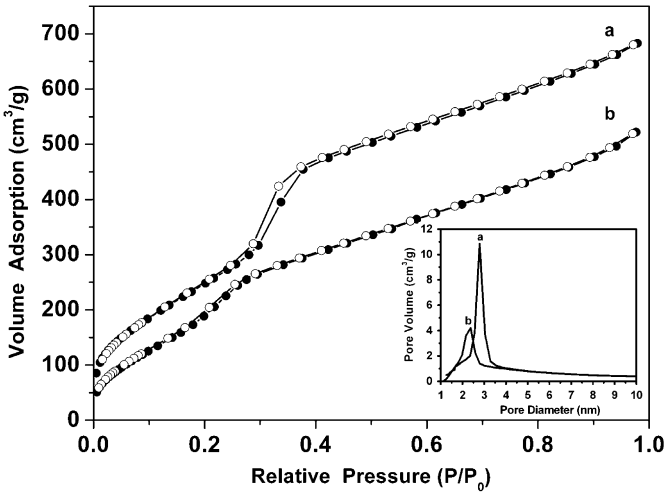

Fig. 4. N_2 adsorption/desorption isotherms of surfactant-extracted phen-MCM-41 (a), and $Tm(DBM)_3$phen-MCM-41 (b) mesoporous materials. The inset shows the BJH pore distributions of phen-MCM-41 (a), and $Tm(DBM)_3$phen-MCM-41 mesoporous materials (b).

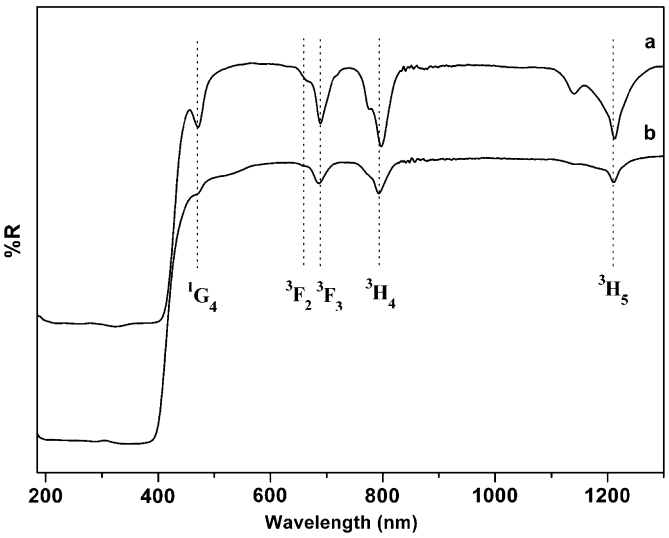

Fig. 5. DR spectra of the $Tm(DBM)_3$phen complex (a) and the $Tm(DBM)_3$phen-MCM-41 mesoporous material (b).

distributions. The textural parameters of the mesoporous materials are summarized in Table 2. It can be clearly seen that the BET surface area, pore volume and pore size decrease from 973 $m^3 g^{-1}$, 1.05 $cm^3 g^{-1}$ and 2.79 nm for surfactant-extracted phen-MCM-41 to 845 $m^3 g^{-1}$, 0.81 $cm^3 g^{-1}$ and 2.37 nm for $Tm(DBM)_3$phen-MCM-41, respectively. This phenomenon is also detected in some literatures [32,33,47]. This is simply due to the presence of the $Tm(DBM)_3$phen complex in the channels of phen-MCM-41. The pore size of $Tm(DBM)_3$phen-MCM-41 mesoporous material estimated by nitrogen adsorption is in agreement with the value observed from TEM images.

3.4. Diffuse reflectance (DR) spectra

The DR of the $Tm(DBM)_3$phen complex and $Tm(DBM)_3$phen-MCM-41 mesoporous material are shown in Fig. 5. In the UV region (200–400 nm) of both curves, a broad absorption band is observed, and can be attributed to electronic transitions from the ground-state level (π) S_0 to the excited level (π^*) S_1 of the organic ligands. The characteristic absorption bands due to the transition from the ground state to the excited states of the Tm^{3+} ion are observed in both curves a and b, where the peaks at 473, 661, 687, 794 and 1208 nm are assigned to $^3H_6 \rightarrow {}^1G_4$, $^3H_6 \rightarrow {}^3F_2$, $^3H_6 \rightarrow {}^3F_3$, $^3H_6 \rightarrow {}^3H_4$ and $^3H_6 \rightarrow {}^3H_5$, respectively. It can be seen that the $Tm(DBM)_3$phen complex and the $Tm(DBM)_3$phen-MCM-41 mesoporous material possess the same position of the absorption onset of the ligands, which together with the appearance of characteristic absorption of Tm^{3+} ion in both curves, suggests that the $Tm(DBM)_3$phen complex is covalently bonded to MCM-41 successfully.

3.5. Photoluminescence studies

The so-called "antenna effect" in lanthanide complexes exhibits in spectrum as the overlaps between the excitation spectrum of complex and the absorption spectra of the ligands. The UV–Vis absorption spectra of DBM and phen in ethanol and the excitation spectrum of bulk $Tm(DBM)_3$phen complex (monitored at 802 nm) are shown in Fig. 6a. The overlaps between the excitation band of $Tm(DBM)_3$phen and the absorption bands that came from ligands DBM and phen can be observed clearly, which

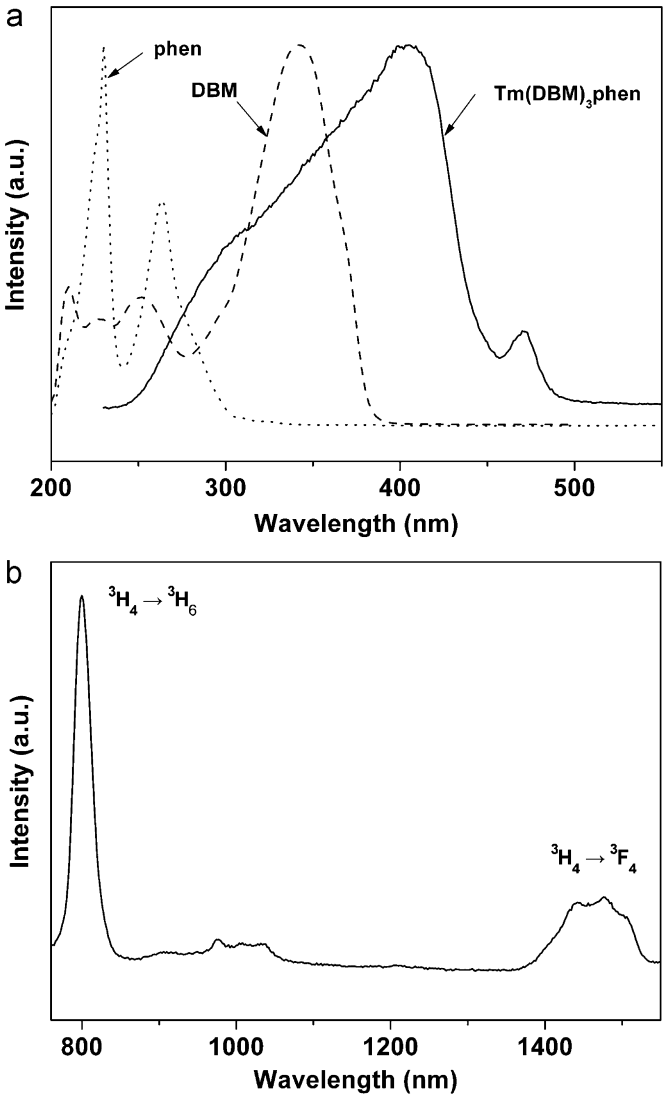

Fig. 6. (a) UV–Vis absorption spectra of DBM and phen in ethanol and the excitation spectrum of $Tm(DBM)_3$phen ($\lambda_{em} = 800$ nm), and (b) emission spectrum of $Tm(DBM)_3$phen complex ($\lambda_{ex} = 400$ nm).

indicates that the central Tm^{3+} ion in $Tm(DBM)_3phen$ can be efficiently sensitized by the ligands, an antenna effect [8–12]. From the Fig. 6a, one can see the overlap between the excitation spectrum of $Tm(DBM)_3phen$ and the absorption spectrum of DBM is larger than the overlap between the excitation spectrum of $Tm(DBM)_3phen$ and the absorption spectrum of phen, which suggests that the antenna effect of DBM is more efficient than that of phen. Consequently, we can come to the conclusion that intramolecular energy transfer in the $Tm(DBM)_3phen$ complex mainly occurs between the DBM ligand and the Tm^{3+} ion [48–50]. In addition, 1,10-phenanthroline can serve as the synergistic agent, since an important issue in the design of lanthanide complexes is to prevent water molecules from binding to the lanthanide ions. With the help of resonant energy transfer, Tm^{3+} ion in $Tm(DBM)_3phen$ complex may accept energy from the lowest triplet states of ligands. In the excitation spectrum of the $Tm(DBM)_3phen$ complex, a broad band ranging from 250 to 450 nm due to the absorption of the ligands superimposed with excitation band originating from the characteristic absorption transition of the Tm^{3+} ion is observed. The *f–f* transition correspond to $^3H_6 \rightarrow {}^1G_4$ (471 nm), which is in agreement with that of the DR spectrum. Upon excitation of the ligands absorption band (400 nm), characteristic Tm^{3+} ion emissions are observed. The emission spectrum displays mainly two bands in the NIR region, 800 ($^3H_4 \rightarrow {}^3H_6$) and 1476 nm ($^3H_4 \rightarrow {}^3F_4$), respectively (see Fig. 6b). It is found that the 1476-nm emission consists of three peaks, which could be ascribed to the Stark splitting of 4*f* electronic levels [5]. To enable a wide gain bandwidth for optical amplification, a broad emission band is desirable [51,52]. In our case, the full width at half maximum (FWHM) of the 1476-nm emission band is 96 nm. Therefore, the 1476-nm emission band of $Tm(DBM)_3phen$ complex is the potential candidate of broadening amplification band from C band (1530–1560 nm) to S^+ band (1450–1500 nm) in optical telecommunication.

The excitation and emission spectra of $Tm(DBM)_3phen$-MCM-41 mesoporous material are shown in Fig. 7. The excitation spectrum of $Tm(DBM)_3phen$-MCM-41 mesoporous material was obtained by monitoring the characteristic emission of the Tm^{3+} ion at 802 nm. After ligand-mediated excitation at 398 nm, the emission spectrum of $Tm(DBM)_3phen$-MCM-41 mesoporous material shows the bands 802 and 1474 nm. The emission bands are assigned to the transition from the excited state $^3H_4$ to the low state $^3H_6$ and $^3F_4$, respectively. The FWHM of the $^3H_4 \rightarrow {}^3F_4$ (1474 nm) transition for $Tm(DBM)_3phen$-MCM-41 mesoporous material is 110 nm, which is broader than that of the $Tm(DBM)_3phen$ complex. Furthermore, compared with those of other Tm-doped materials [5,53], such a broad spectrum enables a wide gain bandwidth for optical amplification. Therefore, the luminescent $Tm(DBM)_3phen$-MCM-41 mesoporous material has the potential to be developed as a broad-band optical amplifier.

The luminescence lifetimes of the $Tm(DBM)_3phen$ complex and $Tm(DBM)_3phen$-MCM-41 mesoporous material were measured at room temperature by using an excitation wavelength of 355 nm and monitored around the most intense emission line (at 800 nm for $Tm(DBM)_3phen$ complex, and at 802 nm for $Tm(DBM)_3phen$-MCM-41 mesoporous material). Both the data are well fitted by a single-exponential function, confirming that Tm^{3+} ions occupy the same average local environment within $Tm(DBM)_3phen$ complex and $Tm(DBM)_3phen$-MCM-41 mesoporous material. The corresponding lifetimes of $Tm(^3H_4)$ excited states are 22 ns and 15 ns, respectively, for $Tm(DBM)_3phen$ and $Tm(DBM)_3phen$-MCM-41. The lower value was observed for $Tm(DBM)_3phen$-MCM-41 compared to that of $Tm(DBM)_3phen$. This may suggest a quenching of NIR luminescence by the vibrations of Si–OH in the pores of $Tm(DBM)_3phen$-MCM-41 mesoporous material.

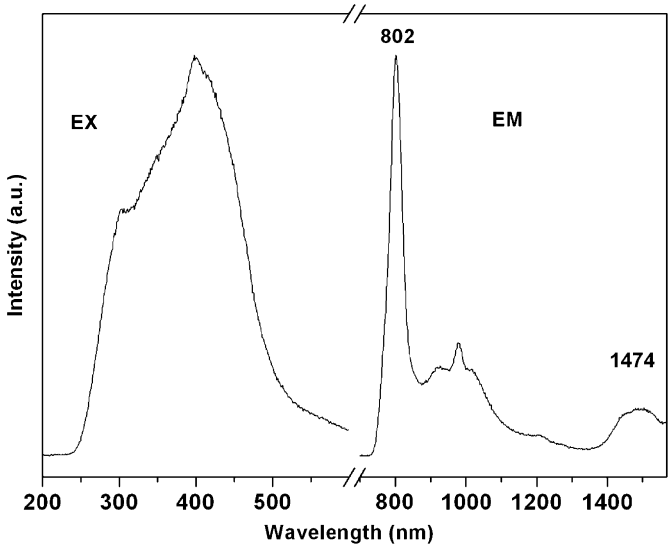

Fig. 7. Excitation and emission spectra of $Tm(DBM)_3phen$-MCM-41 mesoporous material.

4. Conclusions

In summary, the single-crystal X-ray diffraction analyses of the $Tm(DBM)_3phen$ complex has been reported. This thulium complex has been successfully covalently bonded to the ordered MCM-41 mesoporous material by the modified phen group. The optical properties of the $Tm(DBM)_3phen$-MCM-41 mesoporous material were investigated and compared with that of the $Tm(DBM)_3phen$ complex. Of the importance here is the observation of NIR luminescence of Tm^{3+} ion, which centered at 802 and 1474 nm in the $Tm(DBM)_3phen$-MCM-41 mesoporous material. The broad 1474-nm emission band (FWHM = 110 nm) offers the opportunity to develop new material suitable for optical amplifiers operating at 1.5 μm, the telecommunications window.

Acknowledgments

The authors are grateful to the financial aid from the National Natural Science Foundation of China (Grant no. 206301040) and the MOST of China ("973" Program, Grant no. 2006CB601103).

References

[1] N. Sabbatini, M. Guardigli, J.-M. Lehn, Coord. Chem. Rev. 123 (1993) 201.
[2] D. Parker, J.A.G. Williams, J. Chem. Soc. Dalton Trans. (1996) 3613.
[3] M. Elbanowski, B. Makowska, J. Photochem. Photobiol. A 99 (1996) 85.
[4] N. Sabbatini, M. Guardigli, I. Manet, Adv. Photochem. 23 (1997) 213.
[5] F.X. Zang, Z.R. Hong, W.L. Li, M.T. Li, X.Y. Sun, Appl. Phys. Lett. 84 (2004) 2679.
[6] H. Jeong, K. Oh, S.R. Han, T.F. Morse, Chem. Phys. Lett. 367 (2003) 507.
[7] S. Quici, G. Marzanni, A. Forni, G. Accorsi, F. Barigelletti, Inorg. Chem. 43 (2004) 1294.
[8] S.I. Weissman, J. Chem. Phys. 10 (1942) 214.
[9] V. Bekiari, P. Lianos, Adv. Mater. 10 (1998) 1455.
[10] L.D. Carlos, R.A. Sá Ferreira, J.P. Rainho, V. De Zea Bermudez, Adv. Funct. Mater. 12 (2002) 819.
[11] Y. Okamoto, Y. Ueba, N.F. Dzhanibekov, E. Banks, Macromolecules 14 (1981) 17.
[12] N. Sabbatini, A. Mecati, M. Guardigli, V. Balzani, J.M. Lehn, R. Zeissel, R. Ungaro, J. Lumin. 48–49 (1991) 463.
[13] K. Driesen, R. Van Deun, C. Görller-Walrand, K. Binnemans, Chem. Mater. 16 (2004) 1531.
[14] K. Binnemans, P. Lenaerts, K. Driesen, C. Görller-Walrand, J. Mater. Chem. 14 (2004) 191.

[15] A.M. Klonkowski, S. Lis, M. Pietraszkiewicz, Z. Hnatejko, K. Czarnobaj, M. Elbanowski, Chem. Mater. 15 (2003) 656.
[16] C. Sanchez, B. Lebeau, F. Chaput, J.P. Boilot, Adv. Mater. 15 (2003) 1969.
[17] D. Sendor, U. Kynast, Adv. Mater. 14 (2002) 1570.
[18] P. Lenaerts, K. Driesen, R. Van Deun, K. Binnemans, Chem. Mater. 17 (2005) 2148.
[19] K. Kuriki, Y. Koike, Y. Okamoto, Chem. Rev. 102 (2002) 2347.
[20] C.Y. Yang, V. Srdanov, M.R. Robinson, G.C. Bazan, A.J. Heeger, Adv. Mater. 14 (2002) 980.
[21] R. Van Deun, D. Moors, B. De Fré, K. Binnemans, J. Mater. Chem. 13 (2003) 1520.
[22] K. Binnemans, C. Görller-Walrand, Chem. Rev. 102 (2002) 2303.
[23] C.T. Kresge, M.E. Leonowicz, W.J. Roth, J.C. Vartuli, J.S. Beck, Nature 359 (1992) 710.
[24] J.S. Beck, J.C. Vartuli, W.J. Roth, M.E. Leonowicz, C.T. Kresge, K.D. Schmitt, C.T.-W. Chu, D.H. Olson, E.W. Sheppard, S.B. McCullen, J.B. Higgins, J.L. Schlenker, J. Am. Chem. Soc. 114 (1992) 10834.
[25] D.E. De Vos, M. Dams, B.F. Sels, P.A. Jacobs, Chem. Rev. 102 (2002) 3615.
[26] M.E. Davis, Nature 417 (2002) 813.
[27] A. Stein, Adv. Mater. 15 (2003) 763.
[28] B.J. Scott, G. Wirnsberger, G.D. Stucky, Chem. Mater. 13 (2001) 3140.
[29] S. Gago, J.A. Fernandes, J.P. Rainho, R.A. Sá Ferreira, M. Pillinger, A.A. Valente, T.M. Santos, L.D. Carlos, P.J.A. Ribeiro-Claro, I.S. Goncalves, Chem. Mater. 17 (2005) 5077.
[30] H.R. Li, J. Lin, L.S. Fu, J.F. Guo, Q.G. Meng, F.Y. Liu, H.J. Zhang, Microporous Mesoporous Mater. 55 (2002) 103.
[31] C.Y. Peng, H.J. Zhang, J.B. Yu, Q.G. Meng, L.S. Fu, H.R. Li, L.N. Sun, X.M. Guo, J. Phys. Chem. B 109 (2005) 15278.
[32] L.N. Sun, H.J. Zhang, C.Y. Peng, J.B. Yu, Q.G. Meng, L.S. Fu, F.Y. Liu, X.M. Guo, J. Phys. Chem. B 110 (2006) 7249.
[33] L.N. Sun, J.B. Yu, H.J. Zhang, Q.G. Meng, E. Ma, C.Y. Peng, K.Y. Yang, Microporous Mesoporous Mater. 98 (2007) 156.
[34] C.E. Fowler, B. Lebeau, S. Mann, Chem. Commun. (1998) 1825.
[35] J. Feng, H.J. Zhang, C.Y. Peng, J.B. Yu, R.P. Deng, L.N. Sun, X.M. Guo, Microporous Mesoporous Mater. 113 (2008) 402.
[36] Q.G. Meng, P. Boutinand, A.C. Franville, H.J. Zhang, R. Mahiou, Microporous Mesoporous Mater. 65 (2003) 127.
[37] Q.H. Xu, L.S. Li, X.S. Liu, R.R. Xu, Chem. Mater. 14 (2002) 549.
[38] J.-P. Lecomte, A.K.-D. Mesmaeker, M. Demeunynck, J. Lhomme, J. Chem. Soc. Faraday Trans. 89 (1993) 3261.
[39] H.R. Li, J. Lin, H.J. Zhang, L.S. Fu, Q.G. Meng, S.B. Wang, Chem. Mater. 14 (2002) 3651.
[40] D.H. Everett, Pure Appl. Chem. 31 (1972) 577.
[41] M.H. Lim, A. Stein, Chem. Mater. 11 (1999) 3285.
[42] W.H. Zhang, X.B. Lu, J.H. Xiu, Z.L. Hua, L.X. Zhang, M. Robertson, J.L. Shi, D.S. Yan, J.D. Holmes, Adv. Funct. Mater. 14 (2004) 544.
[43] X.M. Guo, L.S. Fu, H.J. Zhang, L.D. Carlos, C.Y. Peng, J.F. Guo, J.B. Yu, R.P. Deng, L.N. Sun, New. J. Chem. 29 (2005) 1351.
[44] M. Kruk, M. Jaroniec, A. Sayari, Langmuir 15 (1997) 6267.
[45] C. Lastokie, K.E. Gubbins, N. Quirke, J. Phys. Chem. 97 (1993) 4786.
[46] P. Selvam, S.K. Bhatia, C.G. Sonwane, Ind. Eng. Chem. Res. 40 (2001) 3237.
[47] M. Sasidharan, N.K. Mal, A. Bhaumik, J. Mater. Chem. 17 (2007) 278.
[48] J.B. Yu, H.J. Zhang, L.S. Fu, R.P. Deng, L. Zhou, H.R. Li, F.Y. Liu, H.L. Fu, Inorg. Chem. Commun. 6 (2003) 852.
[49] L.N. Sun, H.J. Zhang, L.S. Fu, F.Y. Liu, Q.G. Meng, C.Y. Peng, J.B. Yu, Adv. Funct. Mater. 15 (2005) 1041.
[50] L.N. Sun, H.J. Zhang, Q.G. Meng, F.Y. Liu, L.S. Fu, C.Y. Peng, J.B. Yu, G.L. Zheng, S.B. Wang, J. Phys. Chem. B 109 (2005) 6174.
[51] M.P.O. Wolbers, F.C.J.M. van Veggel, B.H.M. Snellink-Ruël, J.W. Hofstraat, F.A.J. Geurts, D.N. Reinhoudt, J. Chem. Soc. Perkin Trans. 2 (1998) 2141.
[52] R. Van Deun, P. Nockemann, C. Görller-Walrand, K. Binnemans, Chem. Phys. Lett. 397 (2004) 447.
[53] E.R. Taylor, L.N. Ng, N.P. Sessions, H. Buuerger, J. Appl. Phys. 92 (2002) 112.